ACES Asian Chemical Editorial Society
DOI: 10.1002/cnma.201900378
CHEMNANOMAT
Minireview

Transforming Noble-Metal Nanocrystals into Complex Nanostructures through Facet-Selective Etching and Deposition

Jaewan Ahn, Luo Zhang, and Dong Qin*[a]

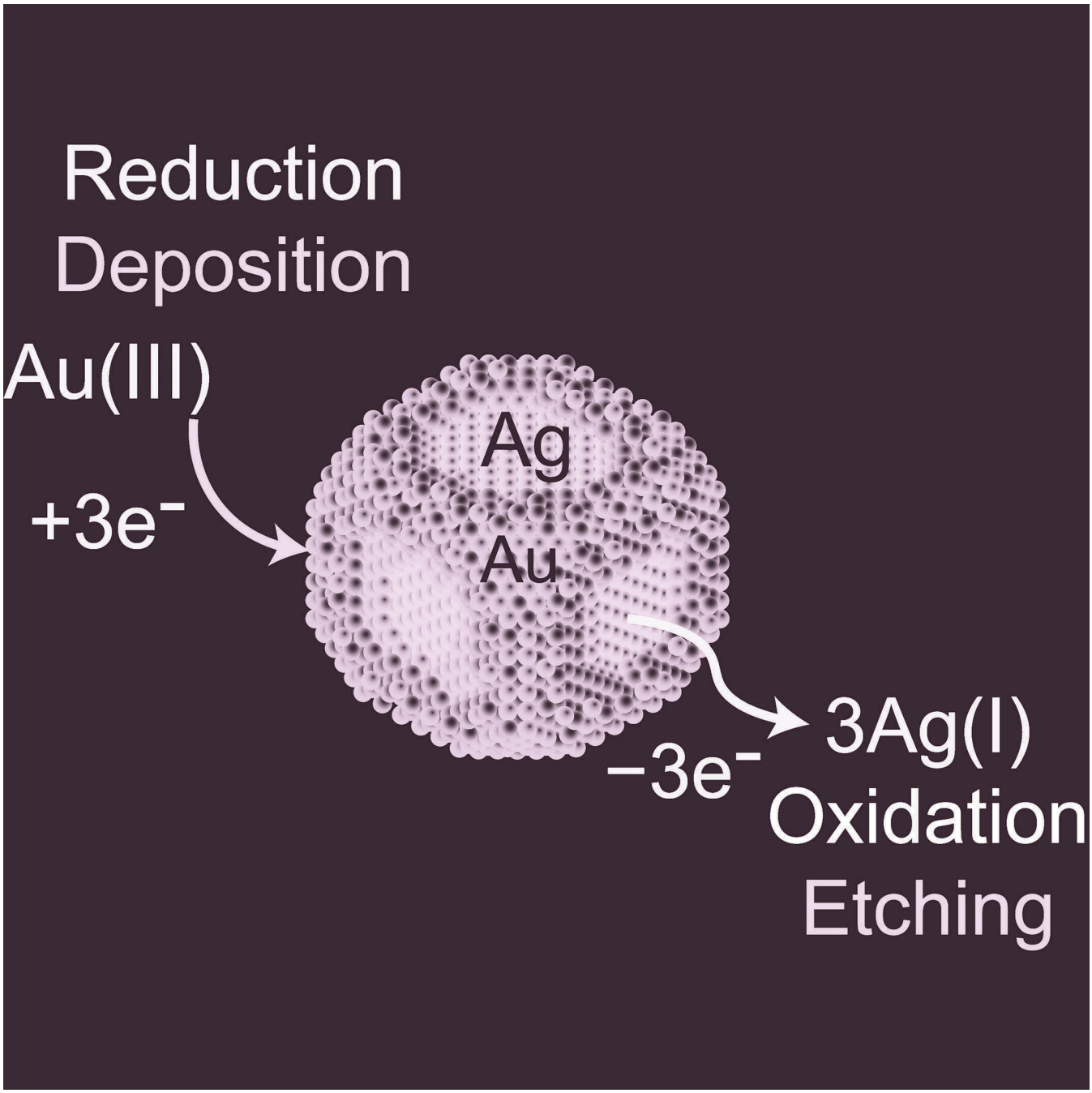

Abstract: Facet-selective etching and deposition, as determined by the landscape of surface energy, represent two powerful methods for the transformation of noble-metal nanocrystals into nanostructures with complex shapes or morphologies. This review highlights the use of these two methods, including integration of them, for the fabrication of novel monometallic and bimetallic nanostructures with enhanced properties. We start with an introduction to the role of surface capping in controlling the facet-selective etching or deposition on the surface of Ag nanocrystals, followed by a case study of how to maneuver etching and deposition at different facets of Pd nanocrystals for the fabrication of nanoframes. We then introduce the use of galvanic replacement to accomplish selective etching and deposition on two different facets in an orthogonal manner, transforming Pd nanocubes into Pd–Pt octapods. By complementing galvanic replacement with a chemical reduction reaction, it is also feasible to control the rates of these two reactions for the conversion of Ag nanocubes into Ag@Ag–Au concave nanocubes and Ag@Au core-shell nanocubes. These transformation methods not only greatly increase the shape diversity of metal nanocrystals but also offer nanocrystals with enhanced plasmonic and/or catalytic properties.

Introduction

Noble-metal nanocrystals have attracted much interest over the past few decades owing to their unique properties that endorse a broad spectrum of applications in photonics/plasmonics[1–4] and catalysis.[5,6] For instance, Au, Ag, and Cu nanocrystals exhibit localized surface plasmon resonance (LSPR) in the visible and near-infrared regions and the frequency can be tuned by varying physical parameters such as composition, size, shape, and structure (solid *vs.* hollow).[7–9] This distinctive light-matter interaction also contributes to the creation of an intense local electrical field on the surface of these nanocrystals, leading to another phenomena known as surface-enhanced Raman scattering (SERS) for ultrasensitive detection.[10–13] On the other hand, it has been documented that the catalytic properties of Pd and Pt nanocrystals could be engineered by controlling their shape and thus the types of facets expressed on the surface.[14–16] It is also feasible to greatly enhance their catalytic activity by introducing high-index facets associated with a concave surface for the presentation of surface atoms with low-coordination numbers in high densities.[17–19]

Two complementary strategies, etching and deposition, have been demonstrated for rationally transforming noble-metal nanocrystals into complex nanostructures.[20] In general, etching refers to an electrochemical process, in which metal atoms are oxidized by an oxidant and dissolved as cations. When the surface atoms are located on distinctive facets of a nanocrystal, they will exhibit different surface energies and thus differ in reactivity.[21] Typically, the atoms with the highest surface energy are most susceptible to etching, giving rise to facet-dependent etching rates for carving a nanocrystal into a unique shape or morphology.[22,23] Alternatively, pre-formed nanocrystals can serve as seeds for the deposition of atomic species through heterogeneous nucleation and growth to attain larger nanocrystals from the same or a different metal.[24–28] The deposition of atomic species is also preferentially initiated from the crystallographic facets with the highest surface energy, leading to faster growth for these facets and their elimination in the final product to minimize the total surface energy. Because the deposited adatoms can diffuse across the surface of a seed during the growth process, one can manipulate the rates of deposition and diffusion to tailor the shape or morphology of the resultant nanocrystal.[29] Significantly, when etching is coupled with deposition, one can remove atoms from some facets while adding atoms to other facets in an orthogonal manner.[30–33] If the rate of etching is greater than that of deposition, a solid nanocrystal can be transformed into a hollow, porous and/or frame structure. In comparison, when growth prevails over etching, the nanocrystal can grow into a larger one with concaved side faces.

As illustrated in Figure 1, this article provides an overview of the strategies that rely on facet-selective etching and/or deposition for transforming nanocrystals into different types of nanostructures, with focus on the mechanistic insights. We start with the first strategy by introducing a number of examples to highlight the importance of surface capping or surface energy in altering the etching or deposition behavior of monometallic nanocrystals for transforming them into nanostructures with more complex shapes or morphologies.[22,34] We further demonstrate that etching can also be coupled with deposition for converting a solid nanocrystal into a hollow, frame-like structure by maneuvering the rates of these two processes.[35] We then discuss the second strategy that leverages galvanic replacement for the fabrication of bimetallic nanocrystals with well-controlled morphologies.[36,37] In an analogy to corrosion, galvanic replacement can be deciphered as a simple redox process, in which oxidation and reduction reactions occur concomitantly at the anode and cathode, respectively. In one case study, galvanic replacement is applied to a Pd nanocube in the presence of halides such of Br^- ions. In the presence of chemisorbed Br^- ions, the {100} facets can serve as an anode for the oxidation of Pd atoms in the form of Pd(II) while the Pt atoms derived from the reduction of Pt(IV) by Pd are deposited on the {111} facets in an orthogonal manner. As a result, the Pd nanocube is gradually transformed into a Pd–Pt octapod.[36] On the other hand, galvanic replacement can be combined with a competing chemical reduction to guide the structural evolution of nanocrystals. As an example, Ag nanocubes were transformed into

[a] *J. Ahn, L. Zhang, Prof. Dr. D. Qin*
School of Materials Science and Engineering
Georgia Institute of Technology
Atlanta, GA 30332 (USA)
E-mail: dong.qin@mse.gatech.edu

Ag@Au–Ag concave nanocubes through selective etching of Ag atoms from the side faces capped by Cl^- ions due to galvanic replacement, accompanied by the deposition of Au atoms at the orthogonal sites such as edges and corners.[38] In parallel, the newly added Au(III) and the dissolved Ag(I) ions can be co-reduced through chemical reduction for the generation of Au and Ag atoms for their co-deposition on the edges and corners. By maneuvering the reaction rates to balance the galvanic replacement with chemical reduction, one can transform the same batch of nanocrystals into nanostructures with different types of complex morphologies.

Facet-Selective Etching *versus* Deposition

Yang and co-workers demonstrated that the landscape of surface energy could be utilized to achieve facet-selective etching of Ag octahedral nanocrystals.[22] Figure 2A shows a schematic diagram illustrating how a Ag octahedron is transformed into a series of nanocrystals with hollow and branched structures by preferentially etching Ag from {100} facets with a weak etchant. In a typical process, a mixture of NH_4OH and H_2O_2 was introduced into an aqueous solution of poly(vinyl pyrrolidone) (PVP) under vigorous stirring at 4 °C, followed by the addition of Ag octahedrons in an ethanol suspension. The etching rates along the {111} and {100} directions could be controlled by varying the concentration of the etchant. Figure 2B shows scanning electron microscopy (SEM) image of the Ag octahedrons. When the concentration of the etchant was low, Figure 2C shows the selective etching of Ag from {111} facets for the generation of nanostructures with hollow side faces. As the concentration of the etchant was increased, Figure 2, D and E, indicates the predominant etching from the {100} facets for the formation of eight distinctive arms and then octapods, respectively. Taken together, it is feasible to select an etchant with an optimal etching power to facilitate facet-selective etching for the fabrication of nanocrystals with complex morphologies and tunable plasmon resonances. It has been demonstrated that these etched particles can serve as sensitive SERS substrates for chemical sensing.

On the other hand, Xia and co-workers explored the use of surface energy in directing facet-selective deposition of Ag cubic nanocrystals. In one study, they demonstrated that the surface energies of {100} and {111} facets on the surface of Ag nanocubes could be maneuvered by introducing ionic species such as Cu(II) to control the deposition of Ag on different types of facets.[34] Figure 3A illustrates the two pathways proposed to account for the evolution of a Ag nanocube into nanocrystals with different morphologies depending on the absence/presence of $Cu(NO_3)_2$ in the reaction solution. In a typical synthesis, aqueous $AgNO_3$ was titrated into an aqueous suspension of Ag nanocubes with slight truncation at corners and then reduced by ascorbic acid (H_2Asc) under ambient conditions. When $Cu(NO_3)_2$ was absent from the reaction solution, the surface energy of {100} facets was greater than that of {111} facets, $\gamma_{(100)} > \gamma_{(111)}$. As such, the Ag atoms derived from the reduction of $AgNO_3$ by H_2Asc were preferentially deposited on {100} to accelerate their growth along $<100>$ directions for the eventual elimination of these facets on the final products.[39] More interestingly, when H_2Asc was used at a sufficiently high concentration, the deposition rate of Ag atoms would surpass the diffusion rate of Ag adatoms, evolving each {100} facet into a concaved surface.[29] Figure 3, B–D, shows SEM images of the products. Alternatively, when $Cu(NO_3)_2$ was present in the reaction system, the Cu(II) ions could selectively cap the {100} facets, reversing the order of the surface energies to $\gamma_{(111)} > \gamma_{(100)}$ and

Dong Qin is an Associate Professor of Materials Science and Engineering at Georgia Institute of Technology, with an adjunct appointment in the School of Chemistry & Biochemistry. Her academic records include a B.S. in Chemistry from Fudan University (1990), a Ph.D. in Physical Chemistry with Professor Hai-Lung Dai from University of Pennsylvania (1996), a postdoctoral stint with Professor George M. Whitesides at Harvard University (1996–1997), and an MBA from the University of Washington (2003). Before joining Georgia Tech in 2012, she held administrative positions as Associate Dean for Research in the School of Engineering and Applied Science at Washington University in St. Louis (2007–2011) and Associate Director of Center for Nanotechnology at the University of Washington (2002–2007). Her current research focuses on the unique properties and applications of nanoscale materials and systems.

Jaewan Ahn is a PhD candidate of Materials Science and Engineering at Georgia Institute of Technology. He received his B.S. in Materials Science and Engineering at Georgia Tech in 2015. His research interests include the shape-controlled synthesis of bimetallic and trimetallic noble metal nanocrystals and the development of a SERS-based platform to investigate the interaction between organic ligands and Ag nanocrystals.

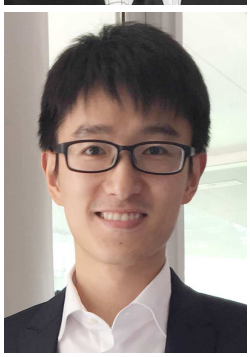

Luo Zhang is a PhD candidate in Marine Materials Science and Engineering at Ocean University of China, and he has been working as visiting PhD student in the Qin Lab at Georgia Institute of Technology from 2017 to 2019. He received his B.S. degree in Materials Science and Engineering from Southwest Jiaotong University in 2013. His research interests include theoretical calculation on crystal growth using density functional theory and rational design and synthesis of noble-metal nanocrystals for plasmonic and catalytic applications.

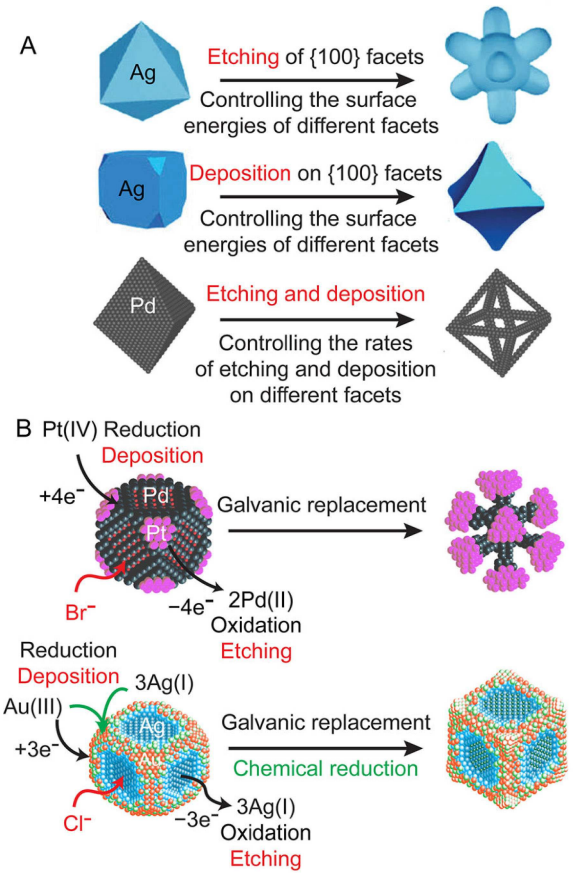

Figure 1. Schematic illustration of two strategies that rely on the etching and deposition for the transformation of nanocrystals into complex nanostructures: (A) facet-selective etching *versus* deposition, as well as an integrated approach for the generation of complex monometallic nanocrystals. (B) galvanic replacement and its combination with a chemical reduction for the fabrication of bimetallic nanostructures with different morphologies. Reprinted with permission from refs 22, 34, 35, 36, and 38. Copyright 2010 American Chemical Society, 2011 Wiley-VCH Verlag GmbH & Co., 2017, 2011, and 2018 American Chemical Society.

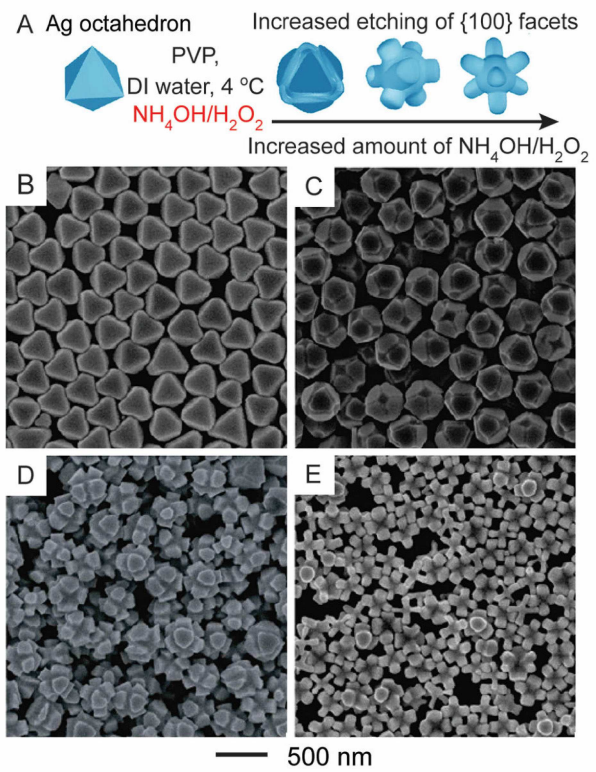

Figure 2. (A) Schematic illustration showing the transformation of a Ag octahedron into various types of nanostructures through selective etching of Ag from the {111} and {100} facets. SEM images of (B) Ag octahedrons and (C–E) the resultant nanostructures after etching with an increased amount of NH_4OH/H_2O_2 in the presence of PVP. Reprinted with permission from ref 22. Copyright 2011 American Chemical Society.

promoting the deposition of Ag on {111} facets. Figure 3, E–G, shows SEM images of the resultant concave cubes, octapods, and trisoctahedrons, respectively. When tested as SERS substrates, the concave octahedrons and trisoctahedrons were more active than the conventional Ag octahedrons with a similar size but covered by flat faces.

With the use of Ag nanoplates, we also investigated facet-selective deposition and etching and identified that these two processes could follow the opposite pathways.[40] Figure 4A shows a schematic illustration describing the transformation of a Ag nanoplate into a twinned cube and its reverse process that involves etching with H_2O_2 locally produced through enzymatic oxidation of glucose. In the first step, citrate-free Ag nanoplates were synthesized and then re-dispersed in an aqueous solution containing H_2Asc and PVP.[41] When aqueous $HAuCl_4$ was introduced, the $AuCl_4^-$ ions could be reduced by both Ag and H_2Asc for the generation of Au atoms through galvanic replacement and chemical reduction, respectively, followed by their deposition on the Ag nanoplates for the production of Ag–Au nanoframes. On the other hand, the Cl^- ions originating from $AuCl_4^-$ could selectively bind to the {100} facets (flat edges) of the Ag nanoplate to lower the surface energy for attaining $\gamma_{(111)} > \gamma_{(100)}$.[42,43] Under this circumstance, upon the titration of $AgNO_3$ into the reaction solution, the Cl^- ions, rather than the Au atoms, directed the deposition of Ag atoms derived from the reduction of $AgNO_3$ by H_2Asc onto {111} facets, transforming Ag nanoplates with a hexagonal shape into twinned cubes with truncated corners. Figure 4, B and D, shows transmission electron microscopy (TEM) images of the products that were obtained at different stages of the growth process.

In the second step, the enzymatically derived H_2O_2 could consecutively remove the Ag atoms located at the two high-energy {111} facets parallel to the twinned plane of the Ag twinned cubes through oxidative etching by following a pathway opposite to deposition. In a typical process, the as-obtained Ag twinned cubes were functionalized with cetyltrimethylammonium chloride (CTAC) to change the surface charge from negative to positive, making it possible to adsorb the negatively charged glucose oxidase (GOx). Because GOx can catalyze the oxidation of glucose by O_2 to produce gluconic acid and H_2O_2,[44–46] one can control the amount of glucose involved in the reaction system to produce enzymatic H_2O_2 on the surface of the particles for the etching of Ag atoms with

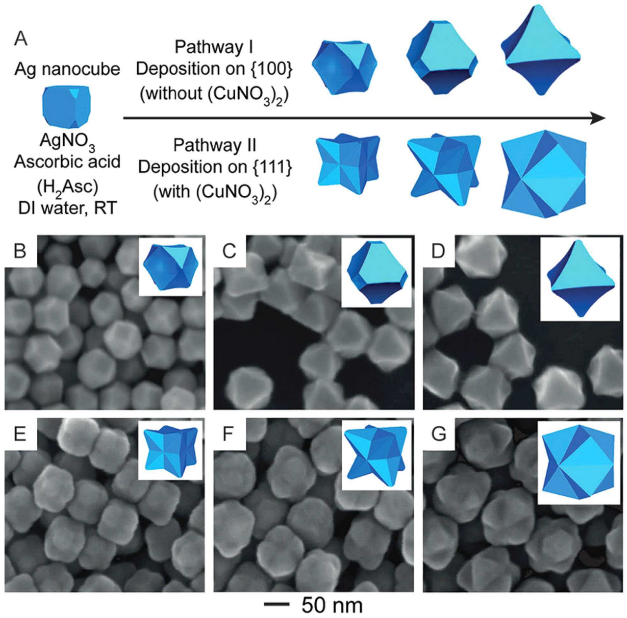

Figure 3. (A) Schematic illustration showing the transformation of a Ag nanocube with truncation at corners into a concave octahedron or a trisoctahedron through selective deposition of Ag on the {100} or {111} facets, respectively. SEM images showing the transformation of Ag nanocubes into (B–D) concave octahedrons and (E–G) trisoctahedrons after adding different amounts of aqueous $AgNO_3$ into a mixture of Ag nanocubes and H_2Asc in the absence and presence of $Cu(NO_3)_2$, respectively. The inset shows a model of the corresponding structure. Reprinted with permission from ref 34. Copyright 2011 Copyright 2012 Wiley-VCH Verlag GmbH & Co.

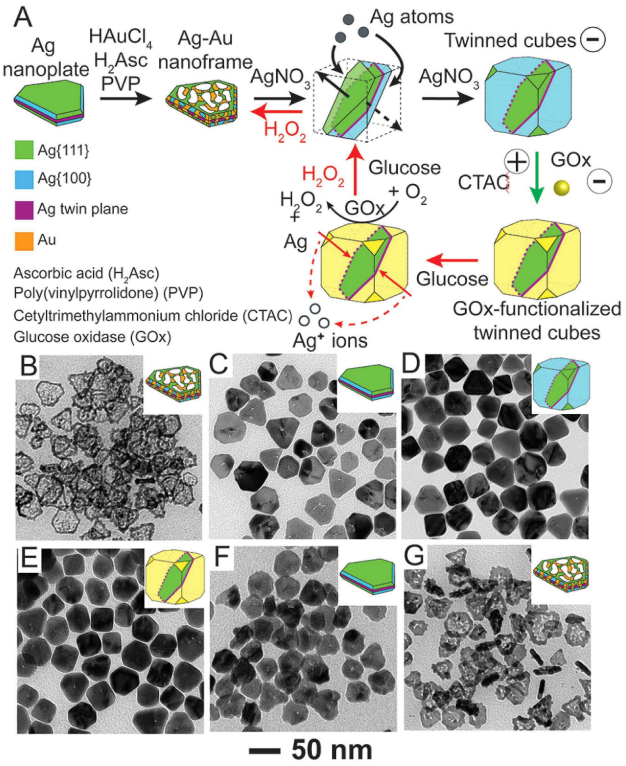

Figure 4. (A) Schematic illustration of site-selected growth of a citrate-free Ag nanoplate into a twinned cube, followed by site-selected etching by enzymatic H_2O_2 along the reversed direction of growth. (B–D) TEM images of the products obtained during the growth of Ag nanoplates in an aqueous solution of $HAuCl_4$, H_2Asc, and PVP, followed by the titration of aqueous $AgNO_3$ at volumes of (B) 0 mL, (C) 0.8 mL, and (D) 1.5 mL, respectively. (E–G) TEM images of (E) GOx-functionalized Ag twinned cubes and two samples after adding the glucose solution at (F) 15 min and (G) 60 min, respectively. The inset shows the corresponding model for each nanocrystal. Reprinted with permission from ref 40. Copyright 2016 American Chemical Society.

selectivity determined by surface energy. As shown in Figure 4E, there was no change to the morphology of the sample before the addition of glucose. Figure 4, F and G, shows TEM images of the particles after the introduction of glucose at time points of 15 and 60 min, respectively, indicating the transformation of twinned cubes into nanoplates and then nanoframes in a sequential manner. Altogether, these results confirm that the growth and etching processes essentially share the same mechanism that relies on the relative surface energies of different facets.

In summary, the facet selective etching versus deposition are two independent processes for the generation of complex nanostructures. It has been demonstrated that both strategies rely on the surface energies of nanocrystal facets to promote either the dissolution of atoms from the original templates or the growth on the nanocrystal seeds, leading to the further increase in the diversity of nanocrystal morphologies for their expanded scope of applications.

Coupling Facet-Selective Etching with Deposition

Despite success through facet-selective etching or deposition, the combination of these two processes opens up new opportunities. For example, Xia reported a method that combined etching with deposition (regrowth) for the transformation of Pd nanocubes of a single size into Pd octahedrons with different edge lengths.[47] A typical experiment was carried out using HCl/O_2 as an oxidative etchant,[48] together with triethylene glycol (Tri-EG) serving as a reducing agent. Because the {100} facets on a Pd nanocube were capped by chemisorbed Br^- ions,[49] Pd atoms were selectively removed from the {111} facets at corner sites during oxidative etching and the resultant Pd(II) ions were then reduced and deposited back onto the nanocube, but preferentially on the {100} facets. By varying the amount of HCl added into the reaction system, it was feasible to control the ratio between the rates for etching and regrowth. At a large amount of HCl, etching was in dominance, resulting in the formation of Pd octahedrons with an edge length about 70% of that of the nanocubes. When HCl was used at a small amount, all the newly formed Pd(II) ions could be reduced and deposited back onto the Pd nanocube. In this case, the resultant Pd octahedron had roughly the same volume as that of the starting nanocube due to the balance between etching and regrowth so that the edge length was about 130% of that of the nanocube. When the amount of HCl

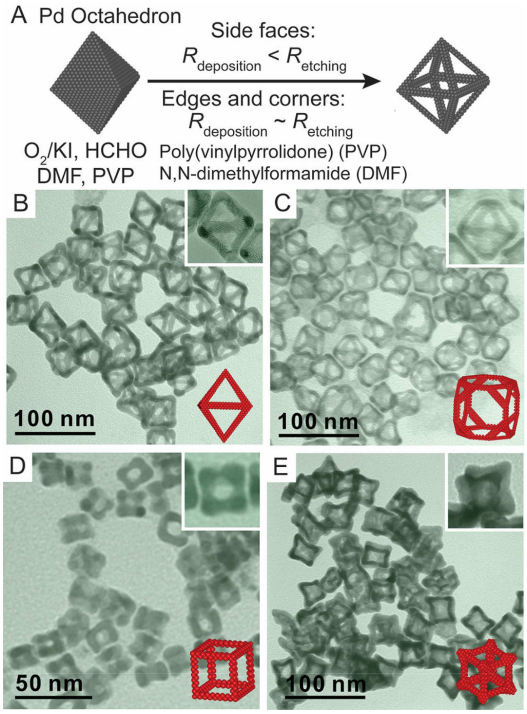

Figure 5. (A) Schematic diagram elucidating the transformation of a Pd octahedron into an octahedral nanoframe as a result of comparable deposition and etching rates along the edges and corners of the octahedron and a higher etching rate along the faces. (C–E) TEM images (with a representative model in the inset) of various types of Pd nanoframes derived from (B) octahedra, (C) cuboctahedra, (D) nanocubes, and (E) concave nanocubes, respectively, using the standard protocol. Reprinted with permission from ref 35. Copyright 2017 American Chemical Society.

was in between, the resultant Pd octahedrons would take an edge length between these two values. This work not only demonstrates the importance of both etching and regrowth in the formation of metal nanocrystals but also offers a simple method for controlling both the shape and size of metal nanocrystals.

Jin, Yin, and co-workers explored the transformation of solid nanocrystals with well-defined shapes into nanoframes by integrating facet-selective etching with deposition.[35] Figure 5A illustrates the mechanism responsible for the generation of an octahedral nanoframe. In a typical synthesis, Pd octahedrons were dispersed in a N,N-dimethylformamide (DMF) solution containing potassium iodide (KI), formaldehyde (HCHO), and PVP. After the reaction vessel was vacuumed and then filled with a certain volume of pure O_2 gas, it was held at 100 °C for 1 h. In the reaction system, the O_2/I^- pair served as an etchant to remove Pd atoms from the octahedron through oxidative etching while HCHO acted as a reducing agent to reduce the dissolved Pd(II) ions back into Pd atoms for their subsequent re-deposition onto the octahedron. By increasing the concentration of HCHO to increase the reducing power, it was possible to maneuver the rates of oxidative etching and deposition, $R_{etching}$ and $R_{deposition}$, on the faces, edges, and corners of the octahedron, respectively. When $R_{deposition}$ became smaller than $R_{etching}$ on the side faces while it was comparable to $R_{etching}$ along the edges and corners, the removal of Pd atoms would be predominantly located on the side faces but largely suppressed at the edges and corners, leading to the conversion of an octahedron into a Pd octahedral nanoframe. In fact, this concept can be applicable to Pd nanocrystals with different shapes. Figure 5, B–E, shows TEM images of the resultant Pd nanoframes that were derived from Pd octahedra, cuboctahedra, nanocubes, and concave nanocubes, respectively. In conclusion, coupling site-selective etching with deposition provides an opportunity to transform solid nanocrystals to nanoframes by simply controlling the rates of etching and deposition on different facets of nanocrystal templates. This facile and versatile approach could become the main stream for the creation of large fraction of atoms on the active sites of nanoframes for applications in catalysis.

Integrating Etching with Deposition through Galvanic Replacement

Galvanic replacement offers another opportunity to integrate oxidative etching with deposition for the transformation of solid nanocrystals of various shapes into complex nanostructures.[50–55] It is an electrochemical process for the deposition of metal *A* on the surface of a template made of a more reactive metal *B*. For example, when Ag nanocubes are mixed with a gold precursor such as $HAuCl_4$ in an aqueous solution, Ag will be dissolved (partially or completely) through oxidation while Au atoms derived from the reduction by Ag will be deposited on the surface of the nanocubes, leading to the production of hollow nanostructures comprised of Ag–Au alloys with tunable LSPR peaks in the range of 500 nm to 1200 nm.[56,57] Likewise, Ag nanocubes could react with Na_2PdCl_4 or K_2PtCl_4 for the generation of Ag–Pd or Ag–Pt bimetallic hollow nanostructures with tunable compositions and interesting catalytic properties.[58–61]

In addition to the fabrication of hollow or porous nanostructures, galvanic replacement has also been explored for the fabrication of bimetallic nanocrystals with a concaved structure. The success relies on the ability to control oxidative etching of atoms from specific facets of nanocrystals while the deposition of another metal would occur on the other facets in an orthogonal manner. To this end, Xia and co-workers demonstrated the transformation of Pd nanocubes into Pd–Pt concave nanocrystals by leveraging the surface capping of Br^- ions toward the {100} facets of Pd nanocubes.[36] In a typical process, as illustrated in Figure 6A, the as-prepared Pd nanocubes are dispersed in an aqueous solution of KBr and PVP, followed by the titration of aqueous H_2PtCl_6 at 90 °C. It was hypothesized that the added Br^- ions would play dual roles in this synthesis. Firstly, Br^- ions would preferentially bind to the {100} facets of the Pd, making these sites more susceptible to dissolution through an oxidation reaction.[49] On the other hand, the Br^- ions would undertake ligand exchange with $PtCl_6^{2-}$ for the formation of $PtBr_6^{2-}$ ions because of the favorable binding constant.[62] Under this circumstance, the Pt atoms derived from the reduction of Pt(IV) by Pd would be deposited on the

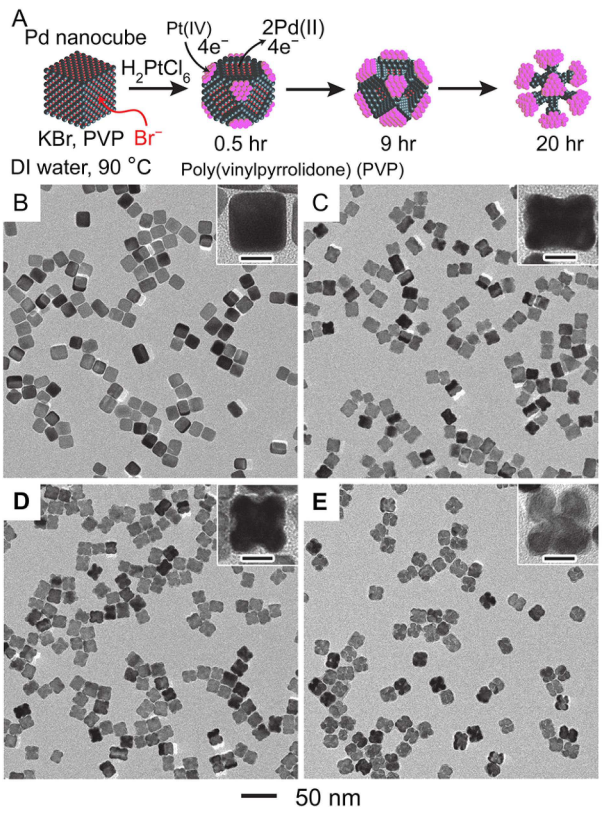

Figure 6. (A) Schematic diagram illustrating the transformation of a Pd nanocube into a Pd–Pt concave nanocube and octapod *via* galvanic replacement reaction between Pd atoms and Pt(IV) ions in the presence of Br^- ions to selectively cap the {100} facets. (B–E) TEM images of the resultant Pd–Pt nanocrystals obtained at (B) 0.5, (C) 4, (D) 9, and (E) 20 h, respectively, after the galvanic replacement reaction was initiated. Scale bars in the insets: 10 nm. Reprinted with permission from ref 36. Copyright 2011 American Chemical Society.

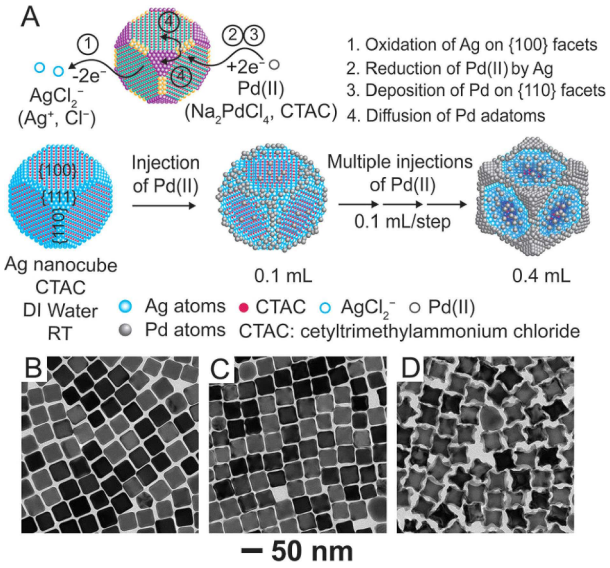

Figure 7. (A) Schematic illustration of the proposed mechanism responsible for the transformation of a Ag nanocube into three different types of Ag–Pd nanostructures *via* reaction with different amounts of Pd(II) precursor in the presence of CTAC. (B–D) TEM images of Ag–Pd concave nanocubes prepared by reacting Ag nanocubes with 0.06 mM Pd(II) precursor solution at volumes of (B) 0.05 mL, (C) 0.1 mL, and (D) 0.4 mL, respectively. Reprinted with permission from ref 37. Copyright 2019 Royal Society of Chemistry.

corners, {111} facets, nanocubes in a fashion orthogonal to etching, leading to the formation of Pd–Pt concave nanocubes. As the replacement reaction continues, the concave nanocubes were further transformed into octapods with concave surfaces. Figure 6, B–E, shows TEM images of the products after Pd nanocubes had reacted with a Pt(IV) precursor for different periods of time. In the early stage, Figure 6B shows that the cubic morphology was essentially preserved but there was a slight change to the degree of corner truncation due to the oxidative etching enabled by the pair of Cl^-/Br^- ions and dissolved O_2 in the reaction solution.[63,64] As the reaction progressed, Figures 6, C and D, shows that the side faces of the nanocubes became more concaved, suggesting the etching of Pd atoms from the {100} facets. At the end, Figure 6E shows the nanostructures after Pd atoms had been extensively removed from the side facets of the nanocubes while the resultant Pt atoms were deposited at the corners. Likewise, the same protocol was also extended to transform Pd octahedra and cuboctahedra into concave nanostructures by selectively etching Pd atoms from the {100} facets as accompanied by the deposition of Pt on the {111} facets in an orthogonal fashion. The Pd–Pt concave nanocubes with different weight percentages of Pt were also evaluated as electrocatalysts for the oxygen reduction reaction (ORR). Remarkably, the sample with 3.4 wt.% of Pt exhibited a large specific electrochemical surface area of 185.8 m^2/g_{Pt} and its mass activity toward ORR was almost four times as great as that of the commercial Pt/C catalyst.

Most recently, we reported the fabrication of Ag–Pd concave nanocubes through site-selected galvanic replacement reaction by following a mechanism similar to the aforementioned Pd–Pt system.[37] Figure 7A illustrates the proposed pathway responsible for the conversion of a Ag nanocube into three different Ag–Pd concave nanocubes with various degree of concaveness on the side faces. Similar to the binding of Br^- ions to the {100} facets of Pd nanocubes, we argue that the Cl^- ions originating from CTAC could selectively bind to the {100} facets on Ag nanocubes,[65] initiating the oxidation of Ag into Ag(I) ions for their release into the reaction solution. The dissolved Ag(I) ions would form soluble $AgCl_2^-$ complex when an excess amount of Cl^- ions was involved in the synthesis.[66] Concomitantly, Pd atoms derived from the reduction of Pd(II) precursor by Ag would be selectively deposited on the edges, the {110} facets with the highest energy, of the nanocube. The Pd adatoms could diffuse across the surface to other regions. By varying the amount of the Pd(II) precursor solution involved in a synthesis, it was possible to carve the Ag atoms from the side faces of nanocubes in a controllable manner. The TEM image in Figure 7B shows that the Ag nanocubes after reacting with 0.05 mL of the 0.06 mM Pd(II) precursor. The cubic shape was well preserved at this stage of reaction. With an increase in the volume of Pd(II) precursor to 0.1 and 0.4 mL, Figure 7, C and D,

shows that Ag nanocubes were transformed into Ag–Pd nanocubes with more significant concaveness on their side faces.

In summary, galvanic replacement reaction allows the integration of oxidative etching with deposition on the individual nanocrystals. It has been demonstrated that the lower surface energy facets could serve as an anode to carve atoms in the form of ions through oxidation while the deposition of metal would proceed in other facets in an orthogonal manner. In turn, galvanic replacement reaction offers a simple approach to produce octapods and concave nanostructures, in addition to its utility to fabricate hollow nanostructures and nanocages.

Complementing Galvanic Replacement with Chemical Reduction

We also introduced a reducing agent to couple with galvanic replacement for the fabrication of bimetallic nanostructures with a concave or a core-shell structure.[38,67] When the rate of galvanic replacement is comparable to that of chemical reduction, Figure 8A illustrates the transformation of a Ag nanocube to a Ag@Au–Ag concave nanocrystal *via* concurrent galvanic etching of the Ag atoms on the side faces and the co-deposition of Ag and Au atoms derived from co-reduction on the edges and corners of the Ag nanocube.[38] In a typical

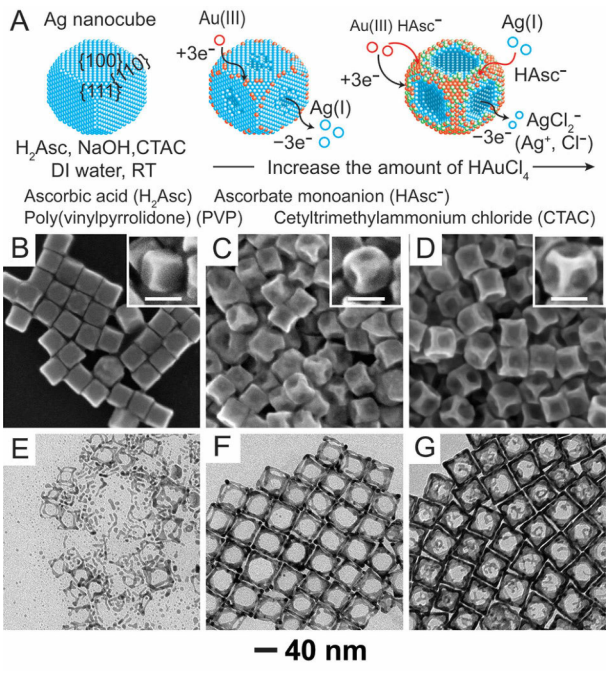

Figure 8. (A) Schematic illustration depicting the transformation of a Ag nanocube into a Ag@Au–Ag concave nanocube in the presence of H_2Asc, NaOH, and CTAC. (B–D) SEM images of the Ag@Au–Ag concave nanocubes prepared by titrating 0.1 mM aqueous $HAuCl_4$ at different volumes of (B) 0.2, (C) 0.8, and (D) 1.6 mL, respectively. (E–G) TEM images of the resultant nanostructures after the removal of Ag from the samples in (B–D) using aqueous H_2O_2. Scale bars in the insets: 40 nm. Reprinted with permission from ref 38. Copyright 2019 American Chemical Society.

experiment, aqueous $HAuCl_4$ was titrated into an aqueous suspension of Ag nanocubes in the presence of H_2Asc, NaOH, and CTAC at an initial pH of 11.6 under ambient conditions. As discussed in the previous case studies, we argue that the Cl^- ions originating from CTAC could preferentially bind to the side faces of Ag nanocubes, making the {100} facets active for the instigation of oxidation of Ag by $AuCl_4^-$. With an excessive amount of Cl^- ions, the dissolved Ag(I) ions would form soluble $AgCl_2^-$ in the reaction solution. Concurrently, both the $AgCl_2^-$ and the Au(III) species were co-reduced by ascorbate monoanion ($HAsc^-$),[68] which was derived from the neutralization between H_2Asc and NaOH, for the generation of Au and Ag atoms. Because the side faces were involved in the galvanic replacement reaction for the dissolution of Ag, the co-deposition of Au and Ag atoms would be initiated at and confined to the edges and corners. By simply increasing the amount of $HAuCl_4$ involved in the reaction, more and more Ag atoms would be carved away from the side faces, leading to the formation of Ag@Au–Ag nanocrystals with increasingly concaved side faces.

Figure 8, B–D, shows SEM images of the nanocrystals obtained after different volumes of 0.1 mM $HAuCl_4$ had been added into the reaction solution. At 0.2 mL, Figure 8B shows a morphology similar to that of the original Ag nanocubes. At 0.8 and 1.6 mL, Figure 8, C and D, shows the resultant nanocubes with an increase in concaveness on the side faces, respectively. After the removal of remaining Ag by etching the above three samples with aqueous H_2O_2, Figure 8, E–G, shows the corresponding nanostructures, indicating the transition from broken nanoframes to cubic nanoframes with an increase in ridge thickness. These results support our argument that Au atoms were deposited on the edges of nanocubes, together with the diffusion of adatoms to the side faces.

Most recently, we developed a strategy for the fabrication of Ag@Au core-shell nanocubes by suppressing the galvanic replacement reaction with a parallel chemical reduction reaction.[67] Figure 9A outlines a proposed pathway for the transformation of a Ag nanocube into a Ag@Au core-shell nanocube. In a typical process, Ag nanocubes were dispersed with PVP in ethylene glycol (EG) at 110 °C, followed by the slow titration of aqueous $HAuCl_4$. In principle, the added $HAuCl_4$ could be reduced by Ag and EG *via* galvanic replacement and chemical reduction, respectively. In the first step, galvanic replacement reaction between $HAuCl_4$ and Ag would enable the deposition of Au on the edges of the nanocubes for the creation of surface defects on the side faces of the nanocubes as the Ag atoms were dissolved to the reaction solution in the form of Ag(I) due to oxidation. In the second step, these defects with high surface energies would become the favored sites for the co-deposition of Ag and Au atoms derived from the co-reduction of both the Ag(I) ions and Au(III) by EG, filling the pits with an Ag–Au alloy to terminate the galvanic replacement reaction in those regions. Starting from this time point, the newly added $HAuCl_4$ would be reduced by EG to Au atoms exclusively, followed by their deposition onto a cubic template for the generation of Au shell in a layer-by-layer fashion. Figure 9B shows TEM image of the product after reacting Ag

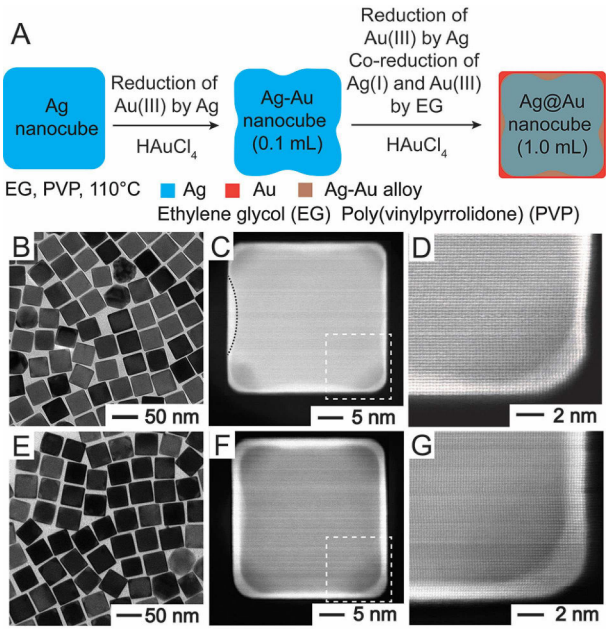

Figure 9. (A) Schematic illustration showing the transformation of a Ag nanocube into a Ag@Au core-shell nanocube in ethylene glycol (EG) held at 110 °C. TEM and HAADF-STEM images of two samples prepared by reacting Ag nanocubes with (B–D) 1.0 and (E–G) 4.0 mL of 0.1 mM aqueous $HAuCl_4$, respectively. Reprinted with permission from ref 67. Copyright 2019 American Chemical Society.

nanocubes with 1.0 mL of 0.1 mM $HAuCl_4$. Figure 9, C and D, shows the aberration-corrected high-angle annular dark-field scanning TEM (HAADF-STEM) images of one nanocube taken from the sample. Based on the contrast between Ag and Au, Figure 9C clearly shows the formation of a core-shell nanocube with a Ag core and a Au shell. In particular, the defects (marked by dotted black line) could be well-defined on the side faces of the Ag nanocubes where the Au atoms tended to be deposited before the conformal deposition of Au atoms would be continued towards the Au shell across the entire surface of the Ag nanocubes. Figure 9D shows the arrangements of Au and Ag atoms, from which we could determine the thickness of the Au layer to be about three atomic layers. When the titration volume of $HAuCl_4$ was increased from 1.0 to 4.0 mL, Figure 9E shows no obvious change in morphology except for an increase in average edge length of for the nanocubes. As shown in Figure 9. F and G, the HAADF-STEM images confirm the formation of eight atomic layers of Au on the surface of the Ag nanocubes. This sample showed remarkable chemical stability in aqueous 30% H_2O_2 for 12 h and an excellent thermal stability in EG solution at 110 °C for 6 h.

In summary, the two competing reactions, namely galvanic replacement reaction and chemical reduction, provide opportunities to fabricate concave hollow nanostructures and core-shell nanocrystals by interplaying the rates of these two reactions. This design rule is applicable to the fabrication of bimetallic or multi-metallic nanocrystals when the reactivity of metal templates is higher than that of the metal being deposited.

Conclusion and Perspectives

We have discussed the use of facet-selective etching and deposition (growth or regrowth) for the transformation of simple nanocrystals such as cubes and octahedrons into nanostructures with complex shapes or morphologies. The facet selectivity for both etching and deposition is largely determined by the landscape of surface energy. In general, etching and growth would be initiated from the facet with the greatest surface energy. By varying the capping agent to manipulate the landscape of surface energy, different types of facets can be selectively activated for either etching or deposition. In the case of galvanic replacement, etching and deposition occur simultaneously at two orthogonal facets with different surface energies. When more than one reaction pathways are involved, such as coupling between galvanic replacement with a chemical reduction, the interplay between these processes makes it possible to achieve a greater control over the morphology of the final products. In this review, we have mainly focused on transformations involving monometallic seeds with simple geometry in order to reveal the insights behind facet selectivity. It should be pointed out that there is also active research in progress regarding the transformation of bimetallic nanocrystals, in which several additional nanoscale processes such as solid-state diffusion,[69] Kirkendall diffusion,[70,71] and dealloying[72,73] other than galvanic replacement could kick in to generate nanocrystals with even more complex shapes, morphologies, and compositions. From all these endeavors, we will surely gain further insights into the facet-selective etching and deposition mechanisms while significantly increase the diversity and functionality of metal nanocrystals. Moving forward, it is important to apply these design rules of metal nanocrystals to other systems such as nanostructures consisting of soft core and hard shell nanoparticles for the construction of multi-shell hollow nanostructures for potential applications in energy storage and conversion.[74]

Acknowledgements

We acknowledge the support from the National Science Foundation (CHE-1708300) and start-up funds from the Georgia Institute of Technology (GT).

Conflict of Interest

The authors declare no conflict of interest.

Keywords: facet-selective deposition · facet-selective etching · galvanic replacement reaction · noble-metal nanocrystals · surface capping

[1] A. J. Haes, S. Zou, G. C. Schatz, R. P. Van Duyne, *J. Phys. Chem. B* **2004**, *108*, 109–116.

[2] S. Eustis, M. A. El-Sayed, *Chem. Soc. Rev.* **2006**, *35*, 209–217.
[3] P. K. Jain, X. Huang, I. H. El-Sayed, M. A. El-Sayed, *Plasmonics* **2007**, *2*, 107–118.
[4] T. K. Sau, A. L. Rogach, F. Jäckel, T. A. Klar, J. Feldmann, *Adv. Mater.* **2010**, *22*, 1805–1825.
[5] C. Burda, X. Chen, R. Narayanan, M. A. El-Sayed, *Chem. Rev.* **2005**, *105*, 1025–1102.
[6] H. Zhang, M. Jin, Y. Xiong, B. Lim, Y. Xia, *Acc. Chem. Res.* **2013**, *46*, 1783–1794.
[7] K. A. Willets, R. P. V. Duyne, *Annu. Rev. Phys. Chem.* **2007**, *58*, 267–297.
[8] Y. Xia, N. J. Halas, *MRS Bull.* **2005**, *30*, 338–348.
[9] E. Ringe, J. M. McMahon, K. Sohn, C. Cobley, Y. Xia, J. Huang, G. C. Schatz, L. D. Marks, R. P. Van Duyne, *J. Phys. Chem. C* **2010**, *114*, 12511–12516.
[10] A. M. Michaels, M. Nirmal, L. E. Brus, *J. Am. Chem. Soc.* **1999**, *121*, 9932–9939.
[11] A. J. Haes, C. L. Haynes, A. D. McFarland, G. C. Schatz, R. P. Van Duyne, S. Zou, *MRS Bull.* **2005**, *30*, 368–375.
[12] B. Sharma, R. R. Frontiera, A.-I. Henry, E. Ringe, R. P. Van Duyne, *Mater. Today* **2012**, *15*, 16–25.
[13] A. B. Zrimsek, N. Chiang, M. Mattei, S. Zaleski, M. O. McAnally, C. T. Chapman, A.-I. Henry, G. C. Schatz, R. P. Van Duyne, *Chem. Rev.* **2017**, *117*, 7583–7613.
[14] S. Mostafa, F. Behafarid, J. R. Croy, L. K. Ono, L. Li, J. C. Yang, A. I. Frenkel, B. R. Cuenya, *J. Am. Chem. Soc.* **2010**, *132*, 15714–15719.
[15] A.-X. Yin, X.-Q. Min, Y.-W. Zhang, C.-H. Yan, *J. Am. Chem. Soc.* **2011**, *133*, 3816–3819.
[16] R. Wang, H. He, L.-C. Liu, H.-X. Dai, Z. Zhao, *Catal. Sci. Technol.* **2012**, *2*, 575–580.
[17] Z. Quan, Y. Wang, J. Fang, *Acc. Chem. Res.* **2013**, *46*, 191–202.
[18] G. Collins, M. Schmidt, C. O'Dwyer, G. McGlacken, J. D. Holmes, *ACS Catal.* **2014**, *4*, 3105–3111.
[19] N. Tian, Z.-Y. Zhou, S.-G. Sun, Y. Ding, Z. L. Wang, *Science* **2007**, *316*, 732.
[20] H. Zhang, M. Jin, Y. Xia, *Angew. Chem. Int. Ed.* **2012**, *51*, 7656–7673.
[21] Z. L. Wang, T. S. Ahmad, M. A. El-Sayed, *Surf. Sci.* **1997**, *380*, 302–310.
[22] M. J. Mulvihill, X. Y. Ling, J. Henzie, P. Yang, *J. Am. Chem. Soc.* **2010**, *132*, 268–274.
[23] Z. Wang, G. Yang, Z. Zhang, M. Jin, Y. Yin, *ACS Nano* **2016**, *10*, 4559–4564.
[24] N. R. Jana, L. Gearheart, C. J. Murphy, *Langmuir* **2001**, *17*, 6782–6786.
[25] B. Nikoobakht, M. A. El-Sayed, *Chem. Mater.* **2003**, *15*, 1957–1962
[26] S. E. Habas, H. Lee, V. Radmilovic, G. A. Somorjai, P. Yang, *Nat. Mater.* **2007**, *6*, 692–697.
[27] Y. Xia, K. D. Gilroy, H.-C. Peng, X. Xia, *Angew. Chem. Int. Ed.* **2017**, *56*, 60–95.
[28] K. D. Gilroy, X. Wang, S. Xie, M. Zhao, D. Qin, Y. Xia, *Adv. Mater.* **2018**, *30*, 1706312.
[29] X. Xia, S. Xie, M. Liu, H.-C. Peng, N. Lu, J. Wang, M. Kim, Y. Xia, *Proc. Natl. Acad. Sci. USA* **2013**, *110*, 6669–6673.
[30] J. Zhang, M. R. Langille, M. L. Personick, K. Zhang, S. Li, C. A. Mirkin, *J. Am. Chem. Soc.* **2010**, *132*, 14012–14014.
[31] E. Villarreal, G. G. Li, H. Wang, *Nanoscale* **2018**, *10*, 18457–18462.
[32] X. Sun, Y. Yang, Z. Zhang, D. Qin, *Chem. Mater.* **2017**, *27*, 4014–4021.
[33] Y. Zhang, J. Ahn, J. Liu, D. Qin, *Chem. Mater.* **2018**, *30*, 2151–2159.
[34] X. Xia, J. Zeng, B. McDearmon, Y. Zheng, Q. Li, Y. Xia, *Angew. Chem. Int. Ed.* **2011**, *50*, 12542–12546.
[35] Z. Wang, H. Wang, Z. Zhang, G. Yang, T. He, Y. Yin, M. Jin, *ACS Nano* **2017**, *11*, 163–170.
[36] H. Zhang, M. Jin, J. Wang, W. Li, P. H. C. Camargo, M. J. Kim, D. Yang, Z. Xie, Y. Xia, *J. Am. Chem. Soc.* **2011**, *133*, 6078–6089.
[37] Z. Luo, J. Ahn, D. Qin, *Nanoscale* **2019**, *11*, 6710–6718.
[38] J. Ahn, D. Wang, Y. Ding, J. Zhang, D. Qin, *ACS Nano* **2018**, *12*, 298–307.
[39] Y. Xia, Y. Xiong, B. Lim, S. E. Skrabalak, *Angew. Chem. Int. Ed.* **2009**, *48*, 60–103.
[40] C.-W. Wang, X. Sun, H.-T. Chang, D. Qin, *Chem. Mater.* **2016**, *28*, 7519–7527.
[41] Q. Zhang, Y. Yang, J. Li, R. Iurilli, S. Xie, D. Qin, *ACS Appl. Mater. Interfaces* **2013**, *5*, 6333–6345.
[42] S. Gómez-Graña, B. Goris, T. Altantzis, C. Fernández-López, E. Carbó-Argibay, A. Guerrero-Martínez, N. Almora-Barrios, N. López, I. Pastoriza-Santos, J. Pérez-Juste, S. Bals, G. Van Tendeloo, L. M. Liz-Marzán, *J. Phys. Chem. Lett.* **2013**, *4*, 2209–2216.
[43] M. H. Kim, S. K. Kwak, S. H. Im, J.-B. Lee, K.-Y. Choi, D.-J. Byun, *J. Mater. Chem. C* **2014**, *2*, 6165–6170.
[44] R. Wilson, A. P. F. Turner, *Biosens. Bioelectron.* **1992**, *7*, 165–185.
[45] H. He, X. Xu, H. Wu, Y. Jin, *Adv. Mater.* **2012**, *24*, 1736–1740.
[46] H. He, X. Xu, H. Wu, Y. Zhai, Y. Jin, *Anal. Chem.* **2013**, *85*, 4546–4553.
[47] M. Liu, Y. Zheng, L. Zhang, L. Guo, Y. Xia, *J. Am. Chem. Soc.* **2013**, *135*, 11752–11755.
[48] Y. Zheng, J. Zeng, A. Ruditskiy, M. Liu, Y. Xia, *Chem. Mater.* **2014**, *26*, 22–33.
[49] H.-C. Peng, S. Xie, J. Park, X. Xia, Y. Xia, *J. Am. Chem. Soc.* **2013**, *135*, 3780–3783.
[50] J. Chen, J. M. McLellan, A. Siekkinen, Y. Xiong, Z.-Y. Li, Y. Xia, *J. Am. Chem. Soc.* **2006**, *128*, 14776–14777.
[51] C. M. Cobley, Y. Xia, *Mater. Sci. Eng. R* **2010**, *70*, 44–62.
[52] C. M. Cobley, Q. Zhang, W. Song, Y. Xia, *Chem. Asian J.* **2011**, *6*, 1479–1484.
[53] X. Lu, H.-Y. Tuan, J. Chen, Z.-Y. Li, B. A. Korgel, Y. Xia, *J. Am. Chem. Soc.* **2007**, *129*, 1733–1742.
[54] X. Xia, Y. Wang, A. Ruditskiy, Y. Xia, *Adv. Mater.* **2013**, *25*, 6313–6333.
[55] X. Hong, D. Wang, S. Cai, H. Rong, Y. Li, *J. Am. Chem. Soc.* **2012**, *134*, 18165–18168.
[56] J. Chen, B. Wiley, Z.-Y. Li, D. Campbell, F. Saeki, H. Cang, L. Au, J. Lee, X. Li, Y. Xia, *Adv. Mater.* **2005**, *17*, 2255–2261.
[57] Y. Yang, Q. Zhang, Z.-W. Fu, D. Qin, *ACS Appl. Mater. Interfaces* **2014**, *6*, 3750–3757.
[58] J. Chen, B. Wiley, J. McLellan, Y. Xiong, Z.-Y. Li, Y. Xia, *Nano Lett.* **2005**, *5*, 2058–2062.
[59] J. W. Hong, S. W. Kang, B.-S. Choi, D. Kim, S. B. Lee, S. W. Han, *ACS Nano*, **2012**, *6*, 2410–2419.
[60] W. Zhang, J. Yang, X. Lu, *ACS Nano*, **2012**, *6*, 7397–7405.
[61] H. Jing, H. Wang, *Chem. Mater.* **2015**, *27*, 2172–2180.
[62] S. C. Srivastava, L. Newman, *Inorg. Chem.* **1966**, *5*, 1506–1510.
[63] D. Seo, C. I. Yoo, I. S. Chung, S. M. Park, S. Ryu, H. Song, *J. Phys. Chem. C* **2008**, *112*, 2469–2475.
[64] Y. Xiong, H. Cai, B. J. Wiley, J. Wang, M. J. Kim, Y. Xia, *J. Am. Chem. Soc.* **2007**, *129*, 3665–3675.
[65] S. Zhou, J. Li, K. D. Gilroy, J. Tao, C. Zhu, X. Yang, X. Sun, Y. Xia, *ACS Nano* **2016**, *10*, 9861–9870.
[66] J. Du, Z. Chen, C. Chen, T. J. Meyer, *J. Am. Chem. Soc.* **2015**, *137*, 3193–3196.
[67] L. Zhang, Y. Zhang, J. Ahn, X. Wang, D. Qin, *Chem. Mater.* **2019**, *31*, 1057–1065.
[68] J. Du, J. J. Cullen, G. R. Buettner, *Biochim. Biophys. Acta Rev. Cancer* **2012**, *1826*, 443–457.
[69] G. G. Li, M. Sun, E. Villarreal, S. Pandey, S. R. Phillpot, H. Wang, *Langmuir* **2018**, *34*, 4340–4350.
[70] E. Gonzalez, J. Arbiol, V. F. Puntes, *Science* **2011**, *334*, 1377–1380.
[71] A. D. Smigelskas, E. O. Kirkendall, *Trans. Am. Inst. Min. Metall. Pet. Eng.* **1947**, *171*, 130–142.
[72] R. C. Newman, K. Sieradzki, *Science* **1994**, *263*, 1708–1709.
[73] J. Erlebacher, M. J. Aziz, A. Karma, N. Dimitrov, K. Sieradzki, *Nature* **2001**, *410*, 410–453.
[74] L. Zhou, Z. Zhuang, H. Zhao, M. Lin, D. Zhao, L. Mai, *Adv. Mater.* **2017**, DOI: 10.1002/adma.201602914.

Manuscript received: June 18, 2019
Accepted manuscript online: July 10, 2019
Version of record online: ■■, ■■■

MINIREVIEW

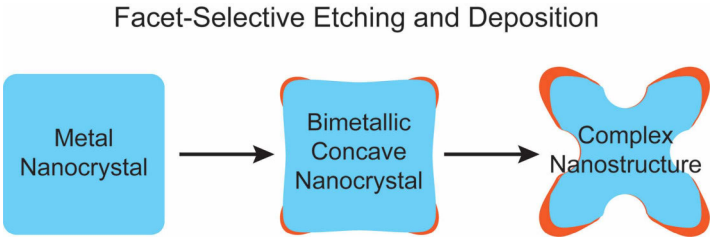

This Minireview discusses the use of facet-selective etching and deposition (growth or regrowth) for the transformation of simple nanocrystals such as cubes and octahedrons into nanostructures with complex shapes or morphologies. When multiple reaction pathways are involved, such as simultaneous galvanic replacement and chemical reduction, the interplay between these processes makes it possible to achieve even greater control over the morphology of the final products.

*J. Ahn, L. Zhang, Prof. Dr. D. Qin**

1 – 11

Transforming Noble-Metal Nanocrystals into Complex Nanostructures through Facet-Selective Etching and Deposition